Diverse mixing states of amine-containing single particles in Nanjing, China

Qi En Zhong[1,2], Chunlei Cheng[1,2]*, Zaihua Wang[3*], Lei Li[1,2], Mei Li[1,2], Dafeng Ge[4,5], Lei Wang[4,5], Yuanyuan Li[4,5], Wei Nie[4,5], Xuguang Chi[4,5], Aijun Ding[4,5], Suxia Yang[2,6], Duohong Chen[7], Zhen Zhou[1,2]

[1]Institute of Mass Spectrometry and Atmospheric Environment, Guangdong Provincial Engineering Research Center for on-line source apportionment system of air pollution, Jinan University, Guangzhou 510632, China

[2]Guangdong-Hongkong-Macau Joint Laboratory of Collaborative Innovation for Environmental Quality, Guangzhou 510632, China

[3]Institute of Resources Utilization and Rare Earth Development, Guangdong Academy of Sciences, Guangzhou 510651, China

[4]Joint International Research Laboratory of Atmospheric and Earth System Sciences (JirLATEST), School of Atmospheric Sciences, Nanjing University, Nanjing 210023, China

[5]Collaborative Innovation Center of Climate Change, Jiangsu Province, Nanjing 210023, China

[6]Institute for Environment and Climate Research, Jinan University, Guangzhou 510632, China

[7]State Environmental Protection Key Laboratory of Regional Air Quality Monitoring, Guangdong Environmental Monitoring Center, Guangzhou 510308, China

*Correspondence to: Chunlei Cheng (chengcl@jnu.edu.cn) and Zaihua Wang (zaihuawang@163.com)

Tel: 86-20-85225991, Fax: 86-20-85225991

Abstract: The mixing states of particulate amines with different chemical components are of great significance in studying the formation and evolution processes of amine-containing particles. In this work, the mixing states of single particles containing trimethylamine (TMA) and diethylamine (DEA) are investigated using a high-performance single-particle aerosol mass spectrometer located in Nanjing, China, in September 2019. TMA- and DEA-containing particles accounted for 22.8% and 5.5% of the total detected single particles, respectively. The particle count and abundance of the TMA-containing particles in total particles notably increased with enhancement of ambient relative humidity (RH), while the DEA-containing particles showed no increase under a high RH. This result suggested the important role of RH in the formation of particulate TMA. Significant enrichments of secondary organic species, including $^{43}C_2H_3O^+$, $^{26}CN^-$, $^{42}CNO^-$, $^{73}C_3H_5O_2^-$, and $^{89}HC_2O_4^-$, were found in DEA-containing particles, indicating that DEA-containing particles were closely associated with the aging of secondary organics. The differential mass spectra of the DEA-containing particles showed much higher abundance of nitrate and organic nitrogen species during the nighttime than during the daytime, which suggested that the nighttime production of particulate DEA might be associated with reactions of gaseous DEA with HNO_3 and/or particulate nitrate. In the daytime the decrease of DEA-containing particles was observed with the enrichment of oxalate and glyoxylate, which suggested a substantial impact of photochemistry on the aging process of DEA-containing particles. Furthermore, greater than 80% of TMA- and DEA-containing particles internally mixed with nitrate, while the abundance of sulfate was higher in the DEA-containing particles (79.3%) than in the TMA-containing particles (55.3%). This suggested that particulate DEA existed both as nitrate and sulfate aminium salts, while the particulate TMA primarily presented as nitrate aminium salt. The different mixing states of the TMA- and DEA-containing particles suggested their different formation processes and various influencing factors, which are difficult to be investigated using bulk analysis. These results provide insights into the discriminated fates of organics during the evolution

process in aerosols, which helps to illustrate the behavior of secondary organic aerosols.

Keywords: Amines; Single particle; Mixing state; Nighttime chemistry; Aminium salts.

1 Introduction

Amines are ubiquitous organic components in aerosols and have a wide range of sources, including animal husbandry, industrial emissions, vehicle exhaust, biomass burning, vegetation emissions, and ocean emissions (Ge et al., 2011b; Facchini et al., 2008; Youn et al., 2015). Due to being highly water-soluble and having strong alkaline properties, amines play an important role in new particle formation and substantially contribute to the secondary organic aerosol (SOA) mass (Zhao et al., 2011; Tao et al., 2016). The formation processes of particulate amines are commonly associated with the gas-to-particle partitioning of gaseous amines and acid-base reactions in the particles (Ge et al., 2011a; Pratt et al., 2009). Therefore, ambient relative humidity (RH) (Rehbein et al., 2011; Zhang et al., 2012), temperature (Huang et al., 2012), particle acidity (Pratt et al., 2009; Rehbein et al., 2011), amine-ammonium exchange (Chan and Chan, 2013; Chu and Chan, 2017; Qiu et al., 2011), and oxidants (Tang et al., 2013; Price et al., 2016) all influence the formation of particulate amines.

Many field observations have been used to investigate the influence of RH on the formation of amines. A high RH is beneficial for the formation of amines in most cases. Zhang et al. (2012) observed a sharp increase in trimethylamine (TMA) during fog events with high RH. Zhou et al. (2019) found that the concentrations of low molecular weight (LMW) amines increased significantly under high RH conditions (> 90%). According to the seasonal distributions of amines during the summer and winter, low temperature was found to be favorable for the partitioning of gaseous amines into particles. Huang et al. (2012) found that the number fraction (N_f) of

amine-containing particles during winter was four times higher than that during summer.

Gaseous amines can react with sulfuric acid, nitric acid, and organic acids to form aminium salts, which underscores the important roles of sulfate and nitrate information of particulate amines (Berndt et al., 2010; Murphy et al., 2007). Berndt et al. (2010) and Wang et al. (2010) found that the formation of aminium salts via a neutralization reaction can affect the growth of particles and the generation of SOAs. Although the concentrations of amines are generally lower than ammonia, the amine-ammonium exchange still contributes to particulate amine formation due to the stronger alkalinity of amines compared to ammonium (Ge et al., 2011b; Sorooshian et al., 2008). Chan et al. (2013) found that the exchange reactions between ammonia and amines showed different reaction rates and product ratios with changes in the aerosol phase state. Qiu et al. (2011) also found that amines can exchange with ammonium to release ammonia. The particulate amines produced from the above pathways and reactions constitute a substantial proportion of the SOAs that impact the physical and chemical properties of fine particles. In addition to the direct contribution of the SOA mass, the oxidation of amines by OH radicals, NO_3 radicals, and O_3 is also a substantial source of SOA production (Price et al., 2016; Tong et al., 2020). Different amines exhibit inconsistent behaviors under the same oxidation environments (NO_3 radicals, OH radicals, or ozone) (Price et al., 2014; Silva et al., 2008; Murphy et al., 2007). In chamber studies, the oxidation of TMA and diethylamine (DEA) by OH vs. NO_3 radicals resulted in different SOA yields, with differences greater than one order of magnitude (Tang et al., 2013). Furthermore, even the same amine showed completely different SOA yields due to OH and NO_3 radical oxidation. Also, the same amine showed distinct trends under the different temperature changing trends. The formation and oxidation processes of particulate amines are not well understood, and these processes require additional comprehensive field observational studies in order to be elucidated.

Most of the field observations did not distinguish between the different behaviors of each type of amine molecule under the same ambient influencing factors. Actually,

due to the different mixing states of amines with other chemical components, the amine molecules typically exhibited different behaviors in terms of being oxidized by OH radicals, forming aminium salts, and altering the hygroscopicity of the particles (Healy et al., 2015; Cheng et al., 2018; Chu et al., 2015; Price et al., 2016). Therefore, the formation processes of the different amines are important to reveal the evolution process of organic aerosols (OAs), and these processes are of great significance to comprehensively understand the influencing factors of OA production.

The mixing states of organics in single particles are commonly investigated by electron microscope and mass spectrometry (Yu et al., 2019; Li et al., 2016a; Cheng et al., 2018). The technique of electron microscope coupled with energy dispersive X-ray spectrometry (EDX) can provide the morphological, physical and some chemical information of organics in single particles (Li et al., 2016b; Li et al., 2021). However, electron microscope coupled with EDX cannot distinguish and identify the specific organic molecules (Li et al., 2016b), which is incapable of analyzing amines in single particles. The technique of single particle mass spectrometry can identify the real-time presence and relative abundance of specific organic ions, which provides substantial data to understand the sources, formation and evolution processes of selective organic markers, providing a feasible approach to investigate the formation processes of different particulate amines (Cheng et al., 2018; Chen et al., 2019; Angelino et al., 2001). Chen et al. (2019) found that high RH was favorable for the uptake of DEA, leading to a DEA-rich substance in the particle phase both during winter and summer. However, Cheng et al. (2018) and Lian et al. (2020) found that RH was not strongly correlated with the formation of amine-containing particles during winter and summer. Pratt et al. (2009) reported that more acidic particles during summer were favorable for the formation of aminium salts compared with the particles present during autumn, indicating that the particle acidity affected the gas to particle partitioning of amines. Rehbein et al. (2011) found more TMA entered the particles as the amount of acidic particles increased. Based on these studies, although the influences of ambient RH and particle acidity on the specific type amines formed

have been reported, yet comparative studies between different amines under the same atmospheric environment using field observation are lacking.

In the present study, the mixing states of TMA- and DEA-containing single particles are investigated during autumn using a high performance single particle aerosol mass spectrometer (HP-SPAMS) located in Nanjing, China. Nanjing is a typical megacity in the Yangtze River Delta (YRD), which is downwind of other megacities including Shanghai, Changzhou, Suzhou, and Wuxi (Figure S1). In addition, Nanjing suffers from heavy loadings of anthropogenic pollutants as well as the complex impacts of biogenic and ship emissions (Xu et al., 2021; Zhao et al., 2020; Ding et al., 2013a). The investigation of mixing states of amines in Nanjing helps to explorer the formation and evolution processes of OAs. Two types of amine-containing particles exhibited different mixing states with secondarily produced OA species. The influences of ambient RH, T, and particle acidity on the mixing states of the two amine-containing particles are evaluated. In addition, the potential heterogeneous formation of DEA during the nighttime is also discussed. The results revealed the distinct chemical behaviors of TMA- and DEA-containing particles and implied the potential role of DEA as an indicator of the aging process of OA.

2 Experimental methods

2.1 Sampling site

Ambient single particles were sampled using the HP-SPAMS from September 2–16, 2019, in Nanjing, China. The campaign was conducted at the Station for Observing Regional Processes of the Earth System (SORPES) station in Nanjing University Xianlin Campus (Ding et al., 2016; Ding et al., 2013a; Ding et al., 2013b; Liu et al., 2021). The instrument was set up on top of a small hill (40 m above the ground) on the Nanjing University campus. The ambient single particles were introduced into the HP-SPAMS through a copper tube.

2.2 Instrumentation of the HP-SPAMS

In this work HP-SPAMS (Hexin Analytical Instrument Co., Ltd., China) was used to detect single particles. The design and principles of SPAMS had previously been described in detail (Li et al., 2011). In short, particles are introduced into the aerodynamic lens through a critical orifice at a flow rate of 75 mL/min (Gong et al., 2021; Li et al., 2011). Individual particles are focused and accelerated to specific velocities, which are detected by two continuous diode Nd:YAG laser beams (532 nm) and then ionized using a pulsed Nd:YAG laser (266 nm). Finally, the z-shaped bipolar time of the flight mass spectrometer is used to detect the generated ions. The improvements and modifications from the SPAMS to the HP-SPAMS are comparatively presented below. The improvement in the SPAMS primarily includes three parts: the application of a concentration device, a delay extraction technology, and a multichannel acquisition technology (Chen et al., 2020; Li et al., 2018). First, the addition of the concentrator increases the injection flow rate by six times, which allows for improved separation of gas and particles. Second, the generated ions from the laser ionization of single particles firstly enter the zone without electric field. Then, the pulsed electric field will be added to accelerate the same kind of ions flying to the detector. This pulsed electric field instead of the constant electric field will prevent the initial deflection of same kind of ions, and the pulsed electric field also provides sufficient energy in the appropriate time to improve the resolutions of positive and negative ions. The mass resolutions of the positive (> 1000 at maximum half width) and negative (> 2000 at maximum half width) ion spectra are then significantly improved. Third, the multichannel acquisition technology is used to divide the signal into two channels, detecting the high and low intensity signals simultaneously without signal loss. This new acquisition technology enables a detectable dynamic signal from 5–20000 mV, which is approximately 40 times higher than that of SPAMS. Generally, the particle size measured by HP-SPAMS ranges from 0.2 to 2.0 μm and was calibrated by polystyrene latex particles before and after the sampling campaign (Li et al., 2011; Li et al., 2018). The field observation result from scanning mobility particle sizer (SMPS) is necessary to scale the measurements of HP-SPAMS to demonstrate the authentic size distributions of specific type particles. Because the SMPS was not

available in this sampling campaign, thus, the size distributions of amine-containing particles were not discussed here.

2.3 Data analysis

The size and chemical compositions of single particles obtained using the HP-SPAMS were analyzed using the Computational Continuation Core (COCO) toolkit in MATLAB software. According to previous studies that have utilized aerosol time-of-flight mass spectrometer (ATOFMS) and SPAMS, the amine-containing particles were identified by querying $^{59}(CH_3)_3N^+$, $^{74}(C_2H_5)_2NH_2^+$, $^{86}(C_2H_5)_2NCH_2^+$, $^{101}(C_2H_5)_3N^+$, $^{102}(C_3H_7)_2NH_2^+$, and $^{143}(C_3H_7)_3N^+$ (Healy et al., 2015; Angelino et al., 2001; Cheng et al., 2018; Zhang et al., 2012). In this work, the marker ions of $^{59}(CH_3)_3N^+$, $^{74}(C_2H_5)_2NH_2^+$, and $^{86}(C_2H_5)_2NCH_2^+$ were detected as the abundant species, and their particle counts and ratios in the total detected single particles are shown in Table 1. Single particles containing $^{86}(C_2H_5)_2NCH_2^+$ only accounted for 3.7% of total particles, which was primarily due to occasional increases on September 5 (Figure S2), possibly due to the outburst of special emissions, such as combustion and industry. Thus, in this work, particles containing $^{59}(CH_3)_3N^+$ and $^{74}(C_2H_5)_2NH_2^+$ were selected to discuss the mixing states and formation processes of the particulate amines. The marker ions of $^{62}NO_3^-$, $^{97}HSO_4^-$, and $^{18}NH_4^+$ were used to identify the nitrate, sulfate, and ammonium in the amine-containing particles (Zhang et al., 2012). Based on field and chamber studies using SPAMS and ATOFMS, the $^{43}C_2H_3O^+$ ion was identified as the representative oxygen-containing organic (Healy et al., 2015; Pratt et al., 2009). The particles containing $^{26}CN^-$ and $^{42}CNO^-$ were considered to be representative of the organic nitrogen-containing particles (Pratt et al., 2011). In addition, the $^{73}C_3H_5O_2^-$ and $^{89}HC_2O_4^-$ ions were designated as glyoxylate and oxalate markers, respectively (Cheng et al., 2017; Zhang et al., 2020). It should be noted that HP-SPAMS measurements cannot provide the quantitative mass concentrations of amines and related chemical species due to the size-dependent transmission efficiencies of particles through aerodynamic lens and composition dependent matrix effect (Cheng et al., 2018; Cheng et al., 2021; Gong et al., 2021). Currently, the

observational results were used to illustrate the distinct impacts of same influencing factors on the behaviors of amine-containing particles.

3 Results and discussion

3.1 Characteristics of amine-containing particles

In this work, the amine-containing particles accounted for 32.1% of total detected single particles, which was higher than in previously reported results for the Pearl River Delta (PRD) region (9.4%–11.1%) and Chongqing (8.3%–12.7%), China. The TMA-containing particles showed a much higher abundance in the total particles (22.8%) than the DEA-containing particles (5.5%) (Table 1), which could have been due to their differential emissions and atmospheric processing (Cheng et al., 2018; Chen et al., 2019; Liu et al., 2020; Ge et al., 2011b). Temporal variations in meteorological parameters, $PM_{2.5}$ concentration, and the count of amine-containing particles are shown in Figure 1. Although the TMA- and DEA-containing particles exhibited similar temporal trends at a lower particle count, their increasing peaks appeared at different periods, suggesting that the reasons for their increase in the particle count were different. Generally, peaks in the DEA-containing particles frequently appeared during the nighttime, which was possibly due to their enhanced source emissions and/or favorable nighttime production (Tang et al., 2013). The ambient RH was relatively high during the entire sampling period (74 ± 14%), especially from September 5–7, when the count of TMA-containing particles sharply increased. However, no obvious enhancement in DEA-containing particles count was found, which suggested other influencing factors on their formation process in addition to the ambient RH.

Additionally, the periods of high concentration of the amine-containing particles were not consistent with the increase in $PM_{2.5}$ concentration, which could have been due to the integrated effects of the emission sources and the secondary formation processes. The gaseous TMA and DEA are mainly from agriculture, industry, vehicle exhaust, biomass combustion, biological, and marine sources (Zhou et al., 2019; Hemmilä et al., 2018; Sintermann et al., 2014; Ge et al., 2011b; Zhang et al., 2017).

Their concentrations vary greatly depending on the influence of source strength near the sampling site. For example, the gaseous concentration of DEA was 14 and 2-5 times higher than TMA in polluted urban areas in China (Yao et al., 2016) and US (You et al., 2014), respectively, while higher concentration of TMA than DEA was observed in the forest site (You et al., 2014). Both the online and offline measurements are difficult to quantitatively resolve their emission sources (You et al., 2014; Yao et al., 2016; Kieloaho et al., 2013; Hellén et al., 2014). Here the backward trajectories of the air masses from sampling site were discussed to explorer their possible different sources. The backward trajectories of the air masses (48 h, 500 m) associated with the spatial distributions of the two amine-containing particles during the entire sampling period (Figure 2). More than 70% of the air masses (Clusters 1 and 4) were from east of the sampling site, which were both connected with anthropogenic emissions in the YRD and marine sources in the East China Sea. TMA-containing particles were primarily from the air masses of Cluster 1 and Cluster 4, while the DEA-containing particles were associated with the air masses of Cluster 3 and Cluster 4, which underwent long-range transport. These results suggested potential different emission sources and atmospheric formation processes of TMA- and DEA-containing particles, which was further investigated by examining their mixing states.

Diurnal variations of TMA- and DEA-containing particles are shown in Figure 3. The particle count of TMA-containing particles and their abundance in the total particles exhibited identical variation patterns. According to molecular characterization of particles from vehicle exhaust, TMA was detected as one of the directly emitted organics from vehicle exhaust (Zhang et al., 2017; Li et al., 2020), which was in accordance with the field studies conducted during traffic hours (Cheng et al., 2018; Chen et al., 2019). Thus, the significant increase of TMA-containing particles in the morning was possibly associated with direct emissions from vehicle exhaust. The DEA-containing particles showed a completely different diurnal pattern compared with the TMA-containing particles. DEA-containing particles increased during nighttime, but sharply decreased during the afternoon, when the

photochemistry was the most active. The nighttime increase could have been due to the high ambient RH and/or enhanced heterogeneous reactions (Zhou et al., 2019; Huang et al., 2012; Zhang et al., 2019). However, since the increase in the DEA-containing particles was not prominent under high RH (Figure 1), enhanced heterogeneous production of particulate DEA could be a more reasonable explanation. The decrease in the DEA-containing particles during the afternoon could have been associated with the photodegradation of DEA and/or repartitioning of particulate DEA under high temperatures during the day (Ge et al., 2011a; Pitts et al., 1978; Murphy et al., 2007). In order to investigate the impact of RH on the formation process of amine-containing particles, the particle counts of amine particles and the relative peak areas (RPAs) of amines in the particles with an increase in the RH are presented in Figure 4. The particle count of TMA-containing particles and the RPA of the TMA showed remarkable increasing trends with an enhancement in RH during the entire sampling period. This result suggested a significant role of RH in the formation of particulate TMA. This was consistent with a field study conducted in Guangzhou, China, which also found an instant increase in TMA-containing particles after the occurrence of fog events (Zhang et al., 2012). In contrast, the particle count of DEA-containing particles only exhibited increased RH range between 70–80% and decreased with the continuous increase in the RH. Additionally, the RPA of the DEA showed little change with an increase in the RH, which suggested the minor influence of a change in RH on the formation of particulate DEA. The different responses of TMA and DEA with RH changes signified their different formation processes in the particles.

3.2 Different mixing states of amine-containing particles

It is important to understand the chemical compositions of amine-containing particles in order to understand their mixing states and track their formation processes. Hence, the positive and negative mass spectra of the amine-containing particles are shown in Figure 5. Generally, TMA- and DEA-containing particles both contained organic fragments such as $^{27}C_2H_3^+$, $^{37}C_3H^+$, $^{43}C_2H_3O^+$, $^{51}C_4H_3^+$, and $^{61}C_5H^+$ in the positive mass spectra. In addition, their negative mass spectra were both characterized

by nitrate, sulfate, and nitric acid ($^{125}H(NO_3)_2^-$). However, DEA-containing particles contained many more organic fragments and a higher abundance of hydrocarbon clusters than the TMA-containing particles. In the positive mass spectra, the abundance of the hydrocarbon fragments with an m/z below 60 was 2–3 times higher in DEA-containing particles than that in TMA-containing particles. In addition, hydrocarbon fragments with an m/z above 60 were barely detectable in TMA-containing particles, while abundant hydrocarbon fragments with an m/z ranging from 60–150 were observed in DEA-containing particles. Furthermore, the DEA-containing particles also contained abundant secondary organic marker ions, including organic nitrogen ($^{26}CN^-$ and $^{42}CNO^-$), acetate ($^{59}C_2H_3O_2^-$), glyoxylate ($^{73}C_3H_5O_2^-$), and oxalate ($^{89}HC_2O_4^-$) in the negative mass spectra, and these were not found in the TMA-containing particles. This was in accordance with the linear regressions between these secondary organic ions containing particles with two amine-containing particles (Table 2), which showed no correlations in the TMA-containing particles ($r^2 < 0.1$), but good correlations in the DEA-containing particles ($r^2 > 0.57$). The differential mass spectral features in the distributions of organics in the two amine-containing particles (Figure 6) suggested that more secondary organics accumulated in DEA-containing particles than in TMA-containing particles. This result also implied that multiple factors influenced the mixing state of DEA-containing particles in addition to ambient RH.

In order to further characterize the mixing states of DEA-containing particles with secondary organic ions, temporal variations and diurnal patterns of secondary organic ions in the DEA-containing particles are presented in Figure 7. As the oxidation products of various organics, the abundances of glyoxylate and oxalate commonly increased between 12:00 and 18:00 (Figure 7), when the photochemistry was most active during the daytime. This result suggested the deep photochemical aging state of DEA-containing particles. This might explain the decrease in the particle counts of DEA-containing particles (Figure 3), which was partially associated with the photo-degradation of particulate DEA. Pitts et al. (1978) reported that under sunlight particulate DEA decomposed to acetamide, while DEA in the gas phase was

oxidized to acetaldehyde, PAN, amide, and imine. Gaseous DEA can be oxidized into carbonyl compounds and other amines by ozone and OH radicals that primarily include acetaldehyde and N-ethylethanimine (Tuazon et al., 2011; Tong et al., 2020). The organic nitrogen markers of $^{26}CN^{-}$ and $^{42}CNO^{-}$ showed different temporal trends with glyoxylate and oxalate. Although the abundances of organic nitrogen markers also increased after 12:00 like oxalate, the markers still maintained high abundances during the nighttime, when glyoxylate and oxalate sharply decreased. This result suggested that the aging process of organics during the nighttime was slower than that during the afternoon in the DEA-containing particles. Thus, the increase of DEA-containing particles (Figure 3) could have been due to the enhanced production of particulate DEA during the nighttime. In addition, the differential mass spectra of DEA-containing particles (Figure 8) between the nighttime (22:00–02:00) and daytime (14:00–18:00) showed a significant enrichment of nitrate during the nighttime. This result suggested that nighttime production of particulate DEA was associated with gaseous HNO_3 and/or particulate nitrate (Price et al., 2016).

Temporal variations in NOx and the N_f of the DEA-containing particles in the total detected particles are presented in Figure 9. They showed similar increasing patterns during the nighttime, and a high abundance of nitrate in the DEA-containing particles was also observed. This result suggested the important role of nitrate in the formation of particulate DEA. The particulate DEA during the nighttime could have been produced from the reaction of gaseous DEA with HNO_3 during the gas phase (R1) followed by the gas to particle partitioning (R2) and/or the direct heterogeneous formation pathway (R3) (Price et al., 2016; Nielsen et al., 2012). The high ambient concentration of NOx is favorable for the production of NO_3 radicals and the heterogeneous production of nitrate, which might explain the distinct enhancement of the DEA-containing particles. However, the same formation pathways were also applied to TMA, yet there was no significant increase in the N_f of the TMA-containing particles in the total particles (Figure 3). This could have been due to the different particle/gas dissociation constant (K_p) for DEA·HNO_3 and TMA·HNO_3, which was several orders of magnitude lower than that for DEA·HNO_3 (7.01E-09)

compared with TMA·HNO_3 (1.65E-06) at 25 ℃ (Price et al., 2016; Ge et al., 2011a). During the entire sampling period, the ambient temperature during the nighttime was approximately 24 ℃. Thus, the produced DEA·HNO_3 tended to stay in the particles, while a portion of the TMA·HNO_3 repartitioned back into the gas phase. This resulted in an insignificant increase in the TMA-containing particles. Further studies should consider the influence of the different volatilities of DEA·HNO_3 and TMA·HNO_3 on the formation of particulate amines in chamber experiments due to the lack of quantitative results in this study.

$$(CH_3CH_2)_2NH_{(g)} + HNO_{3(g)} \rightarrow (CH_3CH_2)_2N \cdot HNO_{3(g)}. \quad (R1)$$

$$(CH_3CH_2)_2N \cdot HNO_{3(g)} \leftrightarrow (CH_3CH_2)_2N \cdot HNO_{3(s)}. \quad (R2)$$

$$(CH_3CH_2)_2NH_{(g)} + NO_3^-{}_{(s)} \rightarrow (CH_3CH_2)_2N \cdot HNO_{3(s)}. \quad (R3)$$

3.3 Formation of aminium salts

To study the acid-base reactions of TMA and DEA with sulfate and nitrate, the N_fs of nitrate-, sulfate-, and ammonium-containing particles in total detected particles and amine-containing particles are shown in Table 3. More than 80% of TMA- and DEA-containing particles internally mixed with nitrate, which was higher than the N_f of nitrate in the total particles (72%). Interestingly, the N_f of sulfate in DEA-containing particles (79.3%) was much higher than that in TMA-containing particles (55.3%) and in the total particles (60.1%). This was similar to a study performed by Lian et al. (2020) that found a stronger correlation between $^{86}(C_2H_5)_2NCH_2^+$ with sulfate than that between TMA and sulfate. In addition, in this work, robust linear correlations ($r^2 > 0.9$) between nitrate-containing particles and amine particles were both observed in TMA- and DEA-containing particles (Table 2). However, a weak linear correlation ($r^2 = 0.32$) was found between the sulfate-containing particles and the TMA-containing particles, while a better linear correlation ($r^2 = 0.86$) was observed in the DEA-containing particles. According to reported studies, the vapor pressure of diethylaminium sulfate (DEAS) ($0.2*10^{-12}$–$12.8*10^{-12}$ Pa) was three orders of magnitude lower than that of trimethylaminium sulfate (TMAS) ($0.6*10^{-9}$–$1.8*10^{-9}$ Pa) at 298 k. In addition, the enthalpy of evaporation was higher than that of TMAS (DEAS: 168 ± 5 kJ mol^{-1}; TMAS: 114 ± 2

kJ mol^{-1}) (Lavi et al., 2013). Therefore, the thermo-stability of DEAS was stronger than TMAS (Qiu and Zhang, 2012), which led to the higher N_f of sulfate in the DEA-containing particles than in the TMA-containing particles.

The N_f of ammonium in DEA-containing particles (13.2%) was lower than in TMA-containing particles (35%) and total particles (19.4%). The low abundance of NH_4^+ in DMA-containing particles had been observed in our previous studies in the PRD region (Cheng et al., 2018), which was partially attributed to the ammonium-amine exchange reactions in the particles. The related laboratory experiments primarily involved the preferential uptake of LMW amines in the H_2SO_4 particles (Sauerwein and Chan, 2017; Chan and Chan, 2013; Chu and Chan, 2017). In this work, the distinct low N_f of NH_4^+ in the DEA particles suggested the possible displacement of NH_4^+ by DEA. Moreover, the higher abundance of sulfate in DEA particles than in TMA particles was more favorable for the occurrence of ammonium-amine exchange reactions in DEA particles. This disparity could imply differential roles of DEA and TMA in the new particle formation process (Wang et al., 2010; Yin et al., 2011; Zhao et al., 2011).

The temporal trends of the N_fs of nitrate-, sulfate-, and ammonium-containing particles in TMA and DEA particles are shown in Figure 10. The N_f of nitrate-containing amine particles exhibited similar variation patterns with each type of amine particle, while the N_f of sulfate-containing amine particles only showed a similar variation pattern with DEA-containing particles. Although aminium nitrate and sulfate salts were both produced in TMA- and DEA-containing particles, the different temporal trends of sulfate and nitrate in the two amine particles suggested that both sulfate and nitrate DEA salts existed in the DEA-containing particles, while nitrate TMA salt dominated in TMA-containing particles (Cheng et al., 2018; Pratt et al., 2009). This difference in the form of aminium salts could signify the potential different influences in the hygroscopic property of secondarily processed particles internally mixing with different amines (Rovelli et al., 2017; Clegg et al., 2013; Lavi et al., 2013). The relative acidity ratio (Ra), defined as the ratio of the sum of the sulfate and nitrate peak areas to the ammonium peak area, has been proposed in field

studies that use single particle mass spectrometry to roughly estimate particle acidity (Huang et al., 2013; Cheng et al., 2018). Although the feasibility of Ra has been supported by the robust linear correlation with authentic particle acidity calculated from mass concentrations of inorganic ions (Huang et al., 2013), this semi-quantitative approach should be carefully treated when it comes to the discussion about the actual acidity of atmospheric particles. In this work, temporal variations in Ra in TMA-containing particles (Ra_1) and DEA-containing particles (Ra_2) are shown in Figure 11. The average Ra_1 was 6.3 ± 1.8 in TMA-containing particles, and Ra_2 was 36.1 ± 21.8 in DEA-containing particles. This result could suggest a more acidic nature of DEA particles than TMA particles. However, after including the peak area of amines (TMA/DEA) in the calculation of Ra, the new Ra′ reduced to 2.1 ± 0.5 in the TMA-containing particles and 6.5 ± 1.2 in the DEA-containing particles. The gap of Ra between the two amine particles significantly decreased after including amines in the calculation. The larger reduction ratio of Ra′ in DEA-containing particles than in TMA-containing particles suggested the effective buffering effect of amines under the absence of ammonium in the particles.

3.4 Implications of the diverse mixing states of amines particles

The mixing states and formation processes of the two amine-containing particles were investigated under the same atmospheric environment, and their different atmospheric behaviors against the same influencing factors suggested their differential contributions to SOA mass. The prominent impact of ambient RH on the formation of particulate TMA suggested a significant role for gas-particle partitioning process to the high water-soluble species in the SOA. However, the slight influence of RH on the formation of the particulate DEA implied the inconsistent role of high RH on the same group of water-soluble organic molecules. In addition, the distinct distribution patterns of secondary organic species in two amine-containing particles also signified that the mixing states of the OA are important to explore their formation processes. Furthermore, the heterogeneous processing of the DEA-containing particles during the nighttime and the photochemical degradation of the DEA during the daytime both generated more fractions of nitrogen- and oxygen-containing species

in the particles than in the TMA-containing particles. This result suggested different roles of particulate TMA and DEA in the evolution of hygroscopicity and aging state of the SOA. In summary, understanding mixing states and formation processes of different amines in single particles is of great significance to reveal the unique response of each type of amine to the same atmospheric environment. Single-particle analysis provided insights into the mixing states of specific organic species to further understand the formation process of the SOA.

4 Summary and conclusions

TMA- and DEA-containing single particles were collected and analyzed on September 2019 using HP-SPAMS in Nanjing, China, and accounted for 22.8% and 5.5% of total detected particles, respectively. The mixing states and formation processes of TMA- and DEA-containing particles were studied. With increased RH, the counts of particulate TMA and the RPA of the TMA displayed an obvious upward trend, while the particle count of the particulate DEA slightly increased when the RH was 70–80%. In addition, the RPA of the DEA showed no difference in reaction to RH change during the entire sampling period. This suggested a differential role for ambient RH during the formation processes of particulate TMA and DEA. The possible formation processes were further evaluated by analyzing the mixing states of the amine-containing particles. The mass spectra of the amine-containing particles showed that the secondary organic species were enriched in the DEA-containing particles. The differential distributions of the secondary ions effectively explained the sharp increase in DEA-containing particles during the nighttime, which could have been due to the heterogeneous reactions of gaseous DEA with HNO_3 and/or nitrate particles. The prominent decrease in the DEA-containing particles during the afternoon was attributed to photo-degradation of particulate DEA. Due to the differences in the thermodynamic properties, the N_f of sulfate in the particulate DEA was higher than that in the particulate TMA. The amine-ammonium exchange reaction resulted in particulate DEA containing less NH_4^+. In addition, the particulate DEA was abundant in sulfate, which was more favorable for the exchange of amine

and ammonium. The higher relative acidity ratio in DEA-containing particles relative to TMA-containing particles could suggest that DEA particles are more acidic. After including the peak area of amines (TMA/DEA) in the calculation, the larger reduction ratio of the Ra′ in DEA-containing particles than in TMA-containing particles suggested the effective buffering effect of amines under the absence of ammonium in the particles. These results revealed the distinct mixing states and chemical behaviors of TMA- and DEA-containing single particles and could imply a potential role for DEA as an indicator of the OA aging process.

Data availability

The observational data, including HP-SPAMS and the meteorological parameters, obtained in this study are available from the corresponding authors upon request (chengcl@jnu.edu.cn).

Author contribution

Qi En Zhong, Chunlei Cheng, Zaihua Wang: methodology, writing original draft. **Dafeng Ge, Lei Wang, Yuanyuan Li, Wei Nie, Xuguang Chi, Aijun Ding:** methodology, sampling. **Lei Li, Mei Li, Suxia Yang, Duohong Chen, Zhen Zhou:** providing discussions and helping to revise original draft.

Competing interests

I declare that I or my co-authors have competing interests as follows: Aijun Ding is editor of ACP.

Acknowledgements: This work was financially supported by the National Key Research and Development Program of China (Grant No. 2018 YFE0106900), the National Natural Science Foundation of China (Grant Nos. 41805093, 41827804 and 41875175), the NSFC of Guangdong Province (Grant No. 2021A1515011206), the

Guangzhou Economic and Technological Development District International Science and Technology Cooperation Project (Grant No. 2018GH08), the National Research Program for Key Issues in Air Pollution Control (Grant No. DQGG0107), the Pearl River Nova Program of Guangzhou (No. 201806010064), and GDAS' Project of Science and Technology Development (2021GDASYL-20210103058).

References

Angelino, S., Suess, D. T., and Prather, K. A.: Formation of aerosol particles from reactions of secondary and tertiary alkylamines: characterization by aerosol time-of-flight mass spectrometry, Environmental science & technology, 35, 3130-3138, 10.1021/es0015444, 2001.

Berndt, T., Stratmann, F., Sipilä, M., Vanhanen, J., Petäjä, T., Mikkilä, J., Grüner, A., Spindler, G., Lee Mauldin Iii, R., Curtius, J., Kulmala, M., and Heintzenberg, J.: Laboratory study on new particle formation from the reaction OH +SO2: influence of experimental conditions, H2O vapour, NH3 and the amine tert-butylamine on the overall process, Atmospheric Chemistry and Physics, 10, 7101-7116, 10.5194/acp-10-7101-2010, 2010.

Chan, L. P. and Chan, C. K.: Role of the aerosol phase state in ammonia/amines exchange reactions, Environmental science & technology, 47, 5755-5762, 10.1021/es4004685, 2013.

Chen, Y., Kozlovskiy, V., Du, X., Lv, J., Nikiforov, S., Yu, J., Kolosov, A., Gao, W., Zhou, Z., Huang, Z., and Li, L.: Increase of the particle hit rate in a laser single-particle mass spectrometer by pulse delayed extraction technology, Atmospheric Measurement Techniques, 13, 941-949, 10.5194/amt-13-941-2020, 2020.

Chen, Y., Tian, M., Huang, R.-J., Shi, G., Wang, H., Peng, C., Cao, J., Wang, Q., Zhang, S., Guo, D., Zhang, L., and Yang, F.: Characterization of urban amine-containing particles in southwestern China: seasonal variation, source, and processing, Atmospheric Chemistry and Physics, 19, 3245-3255, 10.5194/acp-19-3245-2019, 2019.

Cheng, C., Chan, C. K., Lee, B. P., Gen, M., Li, M., Yang, S., Hao, F., Wu, C., Cheng, P., Wu, D., Li, L., Huang, Z., Gao, W., Fu, Z., and Zhou, Z.: Single particle diversity and mixing state of carbonaceous aerosols in Guangzhou, China, The Science of the total environment, 754, 142182, 10.1016/j.scitotenv.2020.142182, 2021.

Cheng, C., Huang, Z., Chan, C. K., Chu, Y., Li, M., Zhang, T., Ou, Y., Chen, D., Cheng, P., Li, L., Gao, W., Huang, Z., Huang, B., Fu, Z., and Zhou, Z.: Characteristics and mixing state of amine-containing particles at a rural site in the Pearl River Delta, China, Atmospheric Chemistry and Physics, 18, 9147-9159, 10.5194/acp-18-9147-2018, 2018.

Cheng, C., Li, M., Chan, C. K., Tong, H., Chen, C., Chen, D., Wu, D., Li, L., Wu, C., Cheng, P., Gao, W., Huang, Z., Li, X., Zhang, Z., Fu, Z., Bi, Y., and Zhou, Z.: Mixing state of oxalic acid containing particles in the rural area of Pearl River Delta, China: implications for the formation mechanism of oxalic acid, Atmospheric Chemistry and Physics, 17, 9519-9533, 10.5194/acp-17-9519-2017, 2017.

Chu, Y. and Chan, C. K.: Reactive Uptake of Dimethylamine by Ammonium Sulfate and Ammonium Sulfate-Sucrose Mixed Particles, The journal of physical chemistry. A, 121, 206-215, 10.1021/acs.jpca.6b10692, 2017.

Chu, Y., Sauerwein, M., and Chan, C. K.: Hygroscopic and phase transition properties of alkyl aminium sulfates at low relative humidities, Physical chemistry chemical physics : PCCP, 17, 19789-19796, 10.1039/c5cp02404h, 2015.

Clegg, S. L., Qiu, C., and Zhang, R.: The deliquescence behaviour, solubilities, and densities of aqueous solutions of five methyl- and ethyl-aminium sulphate salts, Atmospheric Environment, 73, 145-158, 10.1016/j.atmosenv.2013.02.036, 2013.

Ding, A., Nie, W., Huang, X., Chi, X., Sun, J., Kerminen, V.-M., Xu, Z., Guo, W., Petäjä, T., Yang, X., Kulmala, M., and Fu, C.: Long-term observation of air pollution-weather/climate interactions at the SORPES station: a review and outlook, Frontiers of Environmental Science & Engineering, 10, 10.1007/s11783-016-0877-3, 2016.

Ding, A. J., Fu, C. B., Yang, X. Q., Sun, J. N., Zheng, L. F., Xie, Y. N., Herrmann, E., Nie, W., Petäjä, T., Kerminen, V. M., and Kulmala, M.: Ozone and fine particle in the western Yangtze River Delta: an overview of 1 yr data at the SORPES station, Atmospheric Chemistry and Physics, 13, 5813-5830, 10.5194/acp-13-5813-2013, 2013a.

Ding, A. J., Fu, C. B., Yang, X. Q., Sun, J. N., Petäjä, T., Kerminen, V. M., Wang, T., Xie, Y., Herrmann, E., Zheng, L. F., Nie, W., Liu, Q., Wei, X. L., and Kulmala, M.: Intense atmospheric pollution modifies weather: a case of mixed biomass burning with fossil fuel combustion pollution in eastern China, Atmospheric Chemistry and Physics, 13, 10545-10554, 10.5194/acp-13-10545-2013, 2013b.

Facchini, M. C., Decesari, S., Rinaldi, M., Carbone, C., Finessi, E., Mircea, M., Fuzzi, S., Moretti, F., Tagliavini, E., Ceburnis, D., and O'Dowd, C. D.: Important source of marine secondary organic aerosol from biogenic amines, Environmental science & technology, 42, 9116-9121, 10.1021/es8018385, 2008.

Ge, X., Wexler, A. S., and Clegg, S. L.: Atmospheric amines – Part II. Thermodynamic properties and gas/particle partitioning, Atmospheric Environment, 45, 561-577, 10.1016/j.atmosenv.2010.10.013, 2011a.

Ge, X., Wexler, A. S., and Clegg, S. L.: Atmospheric amines – Part I. A review, Atmospheric Environment, 45, 524-546, 10.1016/j.atmosenv.2010.10.012, 2011b.

Gong, H., Cheng, C., Li, M., Yang, S., Zhou, Q., Zhong, Q. E., Zhang, Y., Xie, Y., and Zhou, Z.: The enhanced mixing states of oxalate with metals in single particles in Guangzhou, China, The Science of the total environment, 783, 146962, 10.1016/j.scitotenv.2021.146962, 2021.

Healy, R. M., Evans, G. J., Murphy, M., Sierau, B., Arndt, J., McGillicuddy, E., O'Connor, I. P., Sodeau, J. R., and Wenger, J. C.: Single-particle speciation of alkylamines in ambient aerosol at five European sites, Analytical and bioanalytical chemistry, 407, 5899-5909, 10.1007/s00216-014-8092-1, 2015.

Hellén, H., Kieloaho, A. J., and Hakola, H.: Gas-phase alkyl amines in urban air; comparison with a boreal forest site and importance for local atmospheric chemistry, Atmospheric Environment, 94, 192-197, 10.1016/j.atmosenv.2014.05.029, 2014.

Hemmilä, M., Hellén, H., Virkkula, A., Makkonen, U., Praplan, A. P., Kontkanen, J., Ahonen, L., Kulmala, M., and Hakola, H.: Amines in boreal forest air at SMEAR II station in Finland, Atmospheric Chemistry and Physics, 18, 6367-6380, 10.5194/acp-18-6367-2018, 2018.

Huang, Y., Chen, H., Wang, L., Yang, X., and Chen, J.: Single particle analysis of amines in ambient aerosol in Shanghai, Environmental Chemistry, 9, 202, 10.1071/en11145, 2012.

Huang, Y., Li, L., Li, J., Wang, X., Chen, H., Chen, J., Yang, X., Gross, D. S., Wang, H., Qiao, L., and Chen, C.: A case study of the highly time-resolved evolution of aerosol chemical and optical properties in urban Shanghai, China, Atmospheric Chemistry and Physics, 13, 3931-3944, 10.5194/acp-13-3931-2013, 2013.

Kieloaho, A.-J., Hellén, H., Hakola, H., Manninen, H. E., Nieminen, T., Kulmala, M., and Pihlatie, M.: Gas-phase alkylamines in a boreal Scots pine forest air, Atmospheric Environment, 80, 369-377, 10.1016/j.atmosenv.2013.08.019, 2013.

Lavi, A., Bluvshtein, N., Segre, E., Segev, L., Flores, M., and Rudich, Y.: Thermochemical, Cloud Condensation Nucleation Ability, and Optical Properties of Alkyl Aminium Sulfate Aerosols, The Journal of Physical Chemistry C, 117, 22412-22421, 10.1021/jp403180s, 2013.

Li, L., Liu, L., Xu, L., Li, M., Li, X., Gao, W., Huang, Z., and Cheng, P.: Improvement in the Mass Resolution of Single Particle Mass Spectrometry Using Delayed Ion Extraction, Journal of the American Society for Mass Spectrometry, 29, 2105-2109, 10.1007/s13361-018-2037-4, 2018.

Li, L., Huang, Z., Dong, J., Li, M., Gao, W., Nian, H., Fu, Z., Zhang, G., Bi, X., Cheng, P., and Zhou, Z.: Real time bipolar time-of-flight mass spectrometer for analyzing single aerosol particles, International Journal of Mass Spectrometry, 303, 118-124, 10.1016/j.ijms.2011.01.017, 2011.

Li, W., Liu, L., Zhang, J., Xu, L., Wang, Y., Sun, Y., and Shi, Z.: Microscopic Evidence for Phase Separation of Organic Species and Inorganic Salts in Fine Ambient Aerosol Particles, Environmental science & technology, 55, 2234-2242, 10.1021/acs.est.0c02333, 2021.

Li, W., Shao, L., Zhang, D., Ro, C.-U., Hu, M., Bi, X., Geng, H., Matsuki, A., Niu, H., and Chen, J.: A review of single aerosol particle studies in the atmosphere of East Asia: morphology, mixing state, source, and heterogeneous reactions, Journal of Cleaner Production, 112, 1330-1349, 10.1016/j.jclepro.2015.04.050, 2016a.

Li, W., Sun, J., Xu, L., Shi, Z., Riemer, N., Sun, Y., Fu, P., Zhang, J., Lin, Y., and Wang, X.: A conceptual framework for mixing structures in individual aerosol particles, Journal of Geophysical Research: Atmospheres, 121, 13,784-713,798, 2016b.

Li, X.-J., Shi, X.-W., Ma, Y., and Zheng, J.: Characterization, Seasonal Variation, and Source Apportionments of Particulate Amines ($PM_{2.5}$) in Northern Suburb of Nanjing, Huan Jing ke Xue= Huanjing Kexue, 41, 537-553, 2020.

Liu, Y., Nie, W., Li, Y., Ge, D., Liu, C., Xu, Z., Chen, L., Wang, T., Wang, L., and Sun, P.: Formation of condensable organic vapors from anthropogenic and biogenic VOCs is strongly perturbed by NOx in eastern China, Atmospheric Chemistry and Physics Discussions, 1-44, 2021.

Liu, Z., Chen, H., Li, Q., Sun, J., Wang, L., Yang, X., Xiao, H., Li, M., and Chen, J.: Size‐Resolved Mixing States and Sources of Amine‐Containing Particles in the East China Sea, Journal of Geophysical Research: Atmospheres, 10.1029/2020jd033162, 2020.

Murphy, S., Sorooshian, A., Kroll, J., Ng, N., Chhabra, P., Tong, C., Surratt, J., Knipping, E., Flagan, R., and Seinfeld, J.: Secondary aerosol formation from atmospheric reactions of aliphatic amines, Atmospheric Chemistry and Physics, 7, 2313-2337, 2007.

Nielsen, C. J., Bossi, R., Bunkan, A. J. C., Dithmer, L., Glasius, M., Hallquist, M., Hansen, A. M. K., Lutz, A., Salo, K., and Maguta, M. M.: Atmospheric Degradation of Amines (ADA): summary report from atmospheric chemistry studies of amines, nitrosamines, nitramines and amides, 2012.

Pitts, J. N., Grosjean, D., Van Cauwenberghe, K., Schmid, J. P., and Fitz, D. R.: Photooxidation of aliphatic amines under simulated atmospheric conditions: formation of nitrosamines, nitramines, amides, and photochemical oxidant, Environmental science & technology, 12, 946-953, 10.1021/es60144a009, 1978.

Pratt, K. A., Hatch, L. E., and Prather, K. A.: Seasonal volatility dependence of ambient particle phase amines, Environmental science & technology, 43, 5276-5281, 10.1021/es803189n, 2009.

Pratt, K. A., Murphy, S. M., Subramanian, R., DeMott, P. J., Kok, G. L., Campos, T., Rogers, D. C., Prenni, A. J., Heymsfield, A. J., Seinfeld, J. H., and Prather, K. A.: Flight-based chemical characterization of biomass burning aerosols within two prescribed burn smoke plumes, Atmospheric Chemistry and Physics, 11, 12549-12565, 10.5194/acp-11-12549-2011, 2011.

Price, D. J., Kacarab, M., Cocker, D. R., Purvis-Roberts, K. L., and Silva, P. J.: Effects of temperature on the formation of secondary organic aerosol from amine precursors, Aerosol Science and Technology, 50, 1216-1226, 10.1080/02786826.2016.1236182, 2016.

Price, D. J., Clark, C. H., Tang, X., Cocker, D. R., Purvis-Roberts, K. L., and Silva, P. J.: Proposed chemical mechanisms leading to secondary organic aerosol in the reactions of aliphatic amines with hydroxyl and nitrate radicals, Atmospheric Environment, 96, 135-144, 10.1016/j.atmosenv.2014.07.035, 2014.

Qiu, C. and Zhang, R.: Physiochemical properties of alkylaminium sulfates: hygroscopicity, thermostability, and density, Environmental science & technology, 46, 4474-4480, 10.1021/es3004377, 2012.

Qiu, C., Wang, L., Lal, V., Khalizov, A. F., and Zhang, R.: Heterogeneous reactions of alkylamines with ammonium sulfate and ammonium bisulfate, Environmental science & technology, 45, 4748-4755, 10.1021/es1043112, 2011.

Rehbein, P. J., Jeong, C. H., McGuire, M. L., Yao, X., Corbin, J. C., and Evans, G. J.: Cloud and fog processing enhanced gas-to-particle partitioning of trimethylamine, Environmental science & technology, 45, 4346-4352, 10.1021/es1042113, 2011.

Rovelli, G., Miles, R. E. H., Reid, J. P., and Clegg, S. L.: Hygroscopic properties of aminium sulfate aerosols, Atmospheric Chemistry and Physics, 17, 4369-4385, 10.5194/acp-17-4369-2017, 2017.

Sauerwein, M. and Chan, C. K.: Heterogeneous uptake of ammonia and dimethylamine into sulfuric and oxalic acid particles, Atmospheric Chemistry and Physics, 17, 6323-6339, 10.5194/acp-17-6323-2017, 2017.

Silva, P. J., Erupe, M. E., Price, D., Elias, J., Malloy, Q. G., Li, Q., Warren, B., and Cocker, D. R., 3rd: Trimethylamine as precursor to secondary organic aerosol formation via nitrate radical reaction in the atmosphere, Environmental science & technology, 42, 4689-4696, 10.1021/es703016v, 2008.

Sintermann, J., Schallhart, S., Kajos, M., Jocher, M., Bracher, A., Münger, A., Johnson, D., Neftel, A., and Ruuskanen, T.: Trimethylamine emissions in animal husbandry, Biogeosciences, 11, 5073-5085, 10.5194/bg-11-5073-2014, 2014.

Sorooshian, A., Murphy, S., Hersey, S., Gates, H., Padro, L., Nenes, A., Brechtel, F., Jonsson, H., Flagan, R., and Seinfeld, J.: Comprehensive airborne characterization of aerosol from a major bovine source, Atmospheric Chemistry and Physics, 8, 5489-5520, 2008.

Tang, X., Price, D., Praske, E., Lee, S. A., Shattuck, M. A., Purvis-Roberts, K., Silva, P. J., Asa-Awuku, A., and Cocker, D. R.: NO3 radical, OH radical and O3-initiated secondary aerosol formation from aliphatic amines, Atmospheric Environment, 72, 105-112, 10.1016/j.atmosenv.2013.02.024, 2013.

Tao, Y., Ye, X., Jiang, S., Yang, X., Chen, J., Xie, Y., and Wang, R.: Effects of amines on particle growth observed in new particle formation events, Journal of Geophysical Research: Atmospheres, 121, 324-335, 10.1002/2015jd024245, 2016.

Tong, D., Chen, J., Qin, D., Ji, Y., Li, G., and An, T.: Mechanism of atmospheric organic amines reacted with ozone and implications for the formation of secondary organic aerosols, The Science of the total environment, 737, 139830, 10.1016/j.scitotenv.2020.139830, 2020.

Tuazon, E. C., Martin, P., Aschmann, S. M., Arey, J., and Atkinson, R.: Kinetics of the reactions of OH radicals with 2-methoxy-6-(trifluoromethyl)pyridine, diethylamine, and 1,1,3,3,3-pentamethyldisiloxan-1-ol at 298 ± 2 K, International Journal of Chemical Kinetics, 43, 631-638, 10.1002/kin.20594, 2011.

Wang, L., Lal, V., Khalizov, A. F., and Zhang, R.: Heterogeneous chemistry of alkylamines with sulfuric acid: Implications for atmospheric formation of alkylaminium sulfates, Environmental science & technology, 44, 2461-2465, 2010.

Xu, Z. N., Nie, W., Liu, Y. L., Sun, P., Huang, D. D., Yan, C., Krechmer, J., Ye, P. L., Xu, Z., Qi, X. M., Zhu, C. J., Li, Y. Y., Wang, T. Y., Wang, L., Huang, X., Tang, R. Z., Guo, S., Xiu, G. L., Fu, Q. Y., Worsnop, D., Chi, X. G., and Ding, A. J.: Multifunctional Products of Isoprene Oxidation in Polluted Atmosphere and Their Contribution to SOA, Geophysical Research Letters, 48, 10.1029/2020gl089276, 2021.

Yao, L., Wang, M.-Y., Wang, X.-K., Liu, Y.-J., Chen, H.-F., Zheng, J., Nie, W., Ding, A.-J., Geng, F.-H., Wang, D.-F., Chen, J.-M., Worsnop, D. R., and Wang, L.: Detection of atmospheric gaseous amines and amides by a high-resolution time-of-flight chemical ionization mass spectrometer with protonated ethanol reagent ions, Atmospheric Chemistry and Physics, 16, 14527-14543, 10.5194/acp-16-14527-2016, 2016.

Yin, S., Ge, M., Wang, W., Liu, Z., and Wang, D.: Uptake of gas-phase alkylamines by sulfuric acid, Chinese Science Bulletin, 56, 1241-1245, 10.1007/s11434-010-4331-9, 2011.

You, Y., Kanawade, V. P., de Gouw, J. A., Guenther, A. B., Madronich, S., Sierra-Hernández, M. R., Lawler, M., Smith, J. N., Takahama, S., Ruggeri, G., Koss, A., Olson, K., Baumann, K., Weber, R. J., Nenes, A., Guo, H., Edgerton, E. S., Porcelli, L., Brune, W. H., Goldstein, A. H., and Lee, S. H.: Atmospheric amines and ammonia measured with a chemical ionization mass spectrometer (CIMS), Atmospheric Chemistry and Physics, 14, 12181-12194, 10.5194/acp-14-12181-2014, 2014.

Youn, J. S., Crosbie, E., Maudlin, L. C., Wang, Z., and Sorooshian, A.: Dimethylamine as a major alkyl amine species in particles and cloud water: Observations in semi-arid and coastal regions, Atmos Environ (1994), 122, 250-258, 10.1016/j.atmosenv.2015.09.061, 2015.

Yu, H., Li, W., Zhang, Y., Tunved, P., Dall'Osto, M., Shen, X., Sun, J., Zhang, X., Zhang, J., and Shi, Z.: Organic coating on sulfate and soot particles during late summer in the Svalbard Archipelago, Atmospheric Chemistry and Physics, 19, 10433-10446, 10.5194/acp-19-10433-2019, 2019.

Zhang, G., Bi, X., Chan, L. Y., Li, L., Wang, X., Feng, J., Sheng, G., Fu, J., Li, M., and Zhou, Z.: Enhanced trimethylamine-containing particles during fog events detected by single particle aerosol mass spectrometry in urban Guangzhou, China, Atmospheric Environment, 55, 121-126, 10.1016/j.atmosenv.2012.03.038, 2012.

Zhang, G., Lian, X., Fu, Y., Lin, Q., Li, L., Song, W., Wang, Z., Tang, M., Chen, D., Bi, X., Wang, X., and Sheng, G.: High secondary formation of nitrogen-containing organics (NOCs) and its possible link to oxidized organics and ammonium, Atmospheric Chemistry and Physics, 20, 1469-1481, 10.5194/acp-20-1469-2020, 2020.

Zhang, H., Li, Y., Liu, K., Zhu, L., and Chen, H.: Selective molecular characterization of particulate matter from gasoline cars using internal extractive electrospray ionization mass spectrometry, Analytical Methods, 9, 6491-6498, 10.1039/c7ay02087b, 2017.

Zhang, J., Luo, B., Zhang, W., Rao, Z., and Song, H.: Single-particle characterization of amine-containing particles during summer and winter in Chengdu, CHINA ENVIRONMENTAL SCIENCECE, 39, 3152-3160, 2019.

Zhao, J., Smith, J. N., Eisele, F. L., Chen, M., Kuang, C., and McMurry, P. H.: Observation of neutral sulfuric acid-amine containing clusters in laboratory and ambient measurements, Atmospheric Chemistry and Physics, 11, 10823-10836, 10.5194/acp-11-10823-2011, 2011.

Zhao, J., Zhang, Y., Patton, A. P., Ma, W., Kan, H., Wu, L., Fung, F., Wang, S., Ding, D., and Walker, K.: Projection of ship emissions and their impact on air quality in 2030 in Yangtze River delta, China, Environmental pollution, 263, 114643, 10.1016/j.envpol.2020.114643, 2020.

Zhou, S., Li, H., Yang, T., Chen, Y., Deng, C., Gao, Y., Chen, C., and Xu, J.: Characteristics and sources of aerosol aminiums over the eastern coast of China: insights from the integrated observations in a coastal city, adjacent island and surrounding marginal seas, Atmospheric Chemistry and Physics, 19, 10447-10467, 10.5194/acp-19-10447-2019, 2019.

Tables and figures

Table list:

Table 1. Summary of the major species of detected amine-containing particles and fragments in September in Nanjing, China.

Table 2. The linear correlations (r^2) between secondary ion-containing amine particles within TMA- and DEA-containing particles.

Table 3. Number fractions sulfate, nitrate, and ammonium in TMA-containing particles, DEA-containing particles, and total particles.

Figure caption:

Figure 1. Temporal variations in relative humidity (RH), temperature (T), O_3 concentration, $PM_{2.5}$ concentration, wind speed, wind direction, and TMA- and DEA-containing particles during the entire sampling period.

Figure 2. Backward trajectories (48 h) of air masses at 500 m above the ground during the sampling period: (a) TMA-containing particles counts; (b) DEA-containing particle counts. C1 to C4 represent cluster 1 to cluster 4.

Figure 3. The diurnal variations in particle counts and number fractions of the two amine-containing particles in total particles during the entire sampling period.

Figure 4. Particle counts of amine-containing particles and relative peak area (RPA) of the two amines in single particles, with an increase in ambient RH. (a, c) TMA-containing particles; (b, d) DEA-containing particles.

Figure 5. Mass spectra of TMA- and DEA-containing particles during the entire sampling period.

Figure 6. Differential mass spectra between DEA- and TMA-containing particles.

Figure 7. (a) Temporal trends of the relative peak areas (RPAs) of $^{73}C_3H_5O_2^-$, $^{89}HC_2O_4^-$, $^{26}CN^-$, and $^{42}CNO^-$ in DEA-containing particles. **(b)** Diurnal variations in the relative RPAs of $^{73}C_3H_5O_2^-$, $^{89}HC_2O_4^-$, $^{26}CN^-$, and $^{42}CNO^-$ in DEA-containing particles.

Figure 8. Differential mass spectra of DEA-containing particles between 22:00–02:00 and 14:00–18:00.

Figure 9. Temporal trends of RPA nitrate in DEA-containing particles, number fraction of DEA-containing particles in total particles, and NOx concentration.

Figure 10. Temporal trends of TMA- and DEA-containing particle counts, and number fractions of nitrate, sulfate, and ammonium in TMA- and DEA-containing particles.

Figure 11. Temporal trends of the relative acidity ratios (Ra, Ra$^{'}$) in TMA- and DEA-containing particles.

Tables

Table 1. Summary of the major species of detected amine-containing particles and fragments in September in Nanjing, China.

Alkylamine assignment	Count	Percentage (%)
All detected particles	4 693 931	
$^{59}(CH_3)_3N^+$ (TMA)-containing particles	1072143	22.8
$^{74}(C_2H_5)_2NH_2^+$ (DEA) -containing particles	259913	5.5
$^{86}(C_2H_5)_2NCH_2^+$ (TEA)-containing particles	172621	3.7

Table 2. The linear correlations (r^2) between secondary ion-containing amine particles within TMA- and DEA-containing particles.

	TMA particles	DEA particles
$^{26}CN^-$	0.13	0.70
$^{42}CNO^-$	0.09	0.70
$^{73}C_3H_5O_2^-$	0.01	0.66
$^{89}HC_2O_4^-$	0.09	0.57
$^{43}C_2H_3O^+$	0.05	0.90
$^{62}NO_3^-$	0.93	0.90
$^{97}HSO_4^-$	0.32	0.86
$^{18}NH_4^+$	0.50	0.28

Table 3. Number fractions sulfate, nitrate, and ammonium in TMA-containing particles, DEA-containing particles, and total particles.

	TMA particles	DEA particles	Total particles
Sulfate	55.3	79.3	60.1
Nitrate	81.6	81.8	72.0
Ammonium	35.0	13.2	19.4

Figures

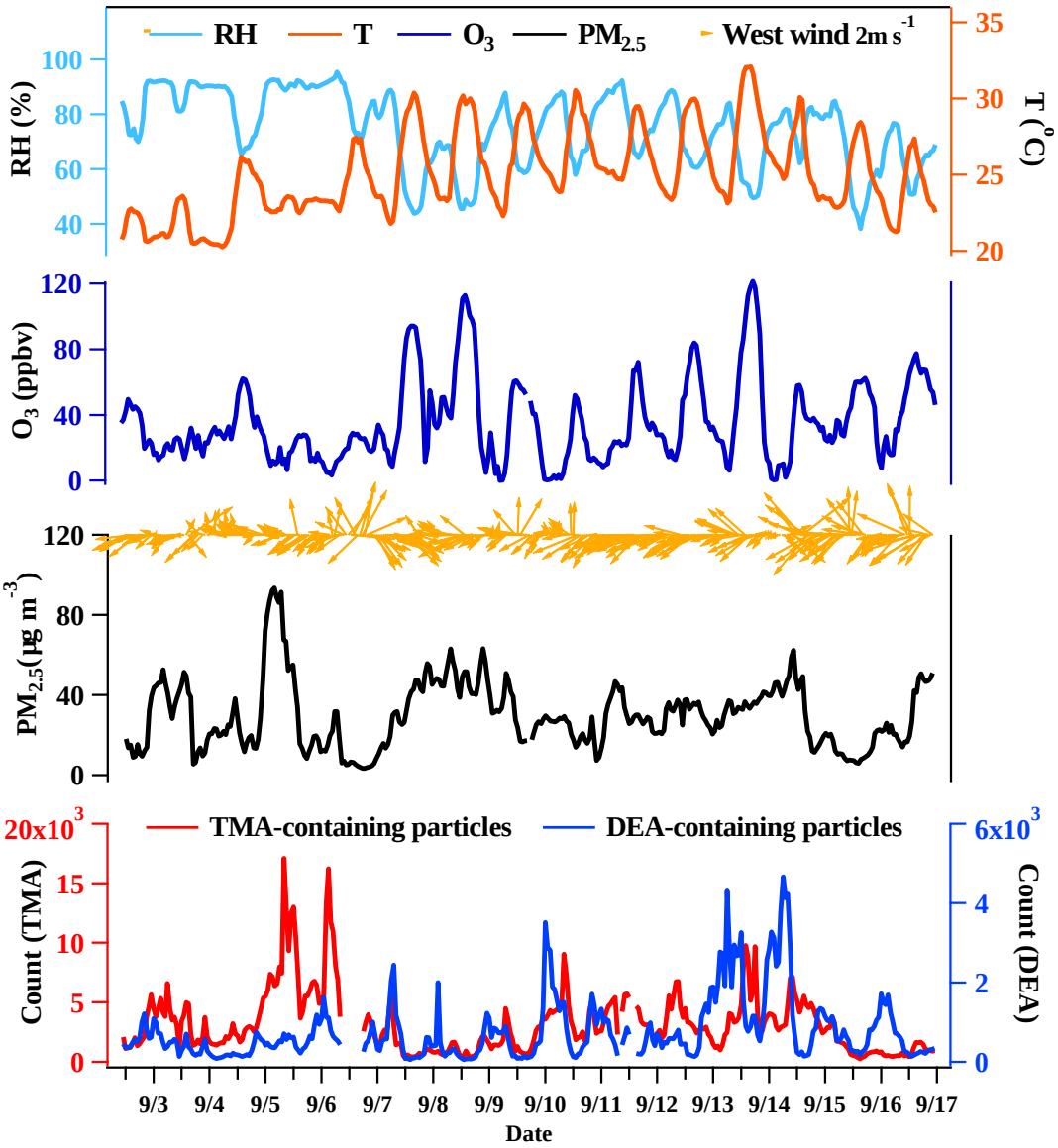

Figure 1. Temporal variations in relative humidity (RH), temperature (T), O_3 concentration, $PM_{2.5}$ concentration, wind speed, wind direction, and TMA- and DEA-containing particles during the entire sampling period.

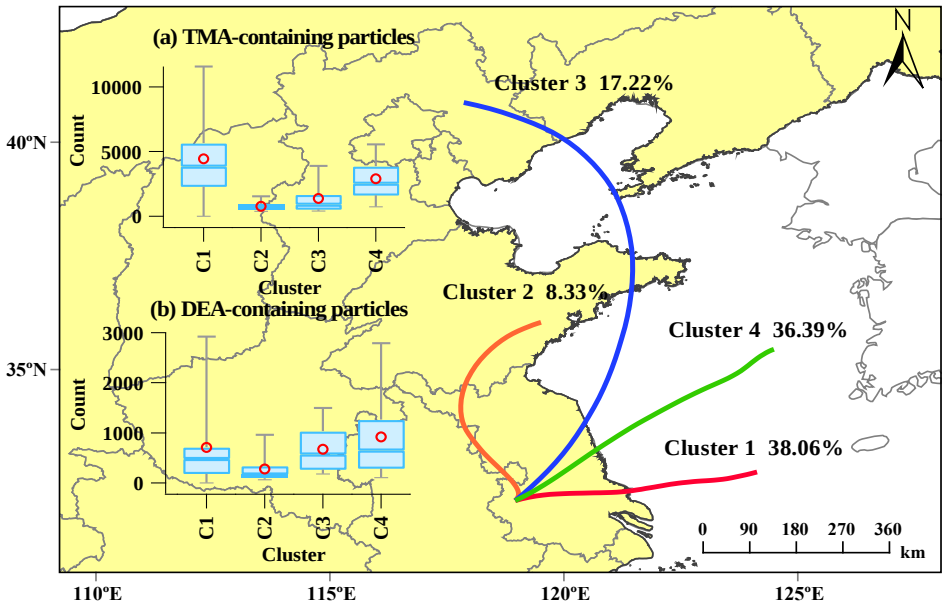

Figure 2. Backward trajectories (48 h) of air masses at 500 m above the ground during the sampling period: (a) TMA-containing particles counts; (b) DEA-containing particle counts. C1 to C4 represent cluster 1 to cluster 4.

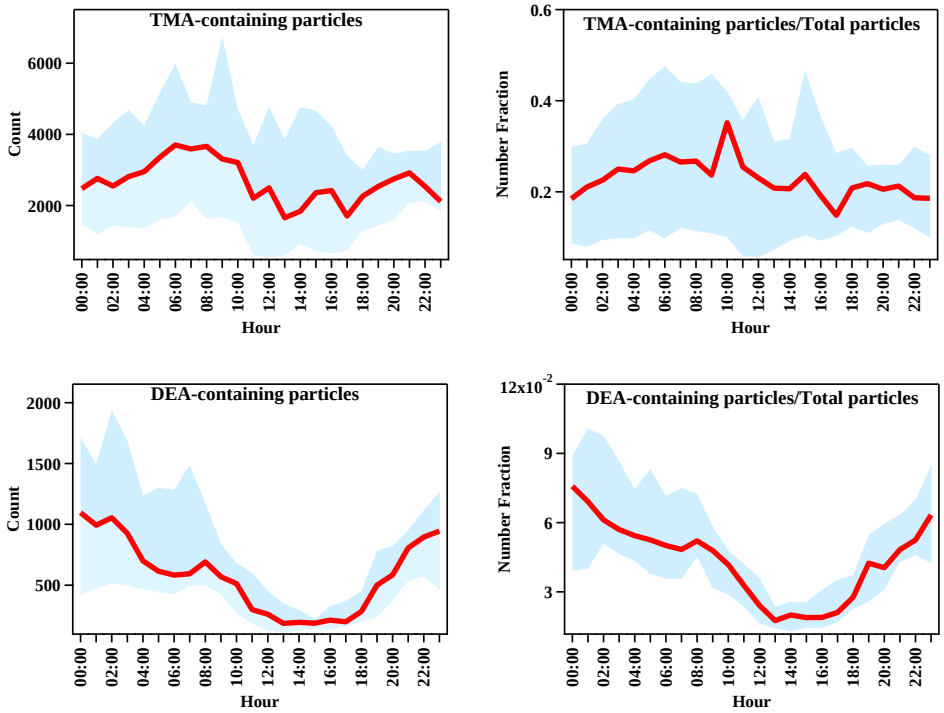

Figure 3. The diurnal variations in particle counts and number fractions of the two amine-containing particles in total particles during the entire sampling period. The shaded areas represent the 75th and 25th percentiles.

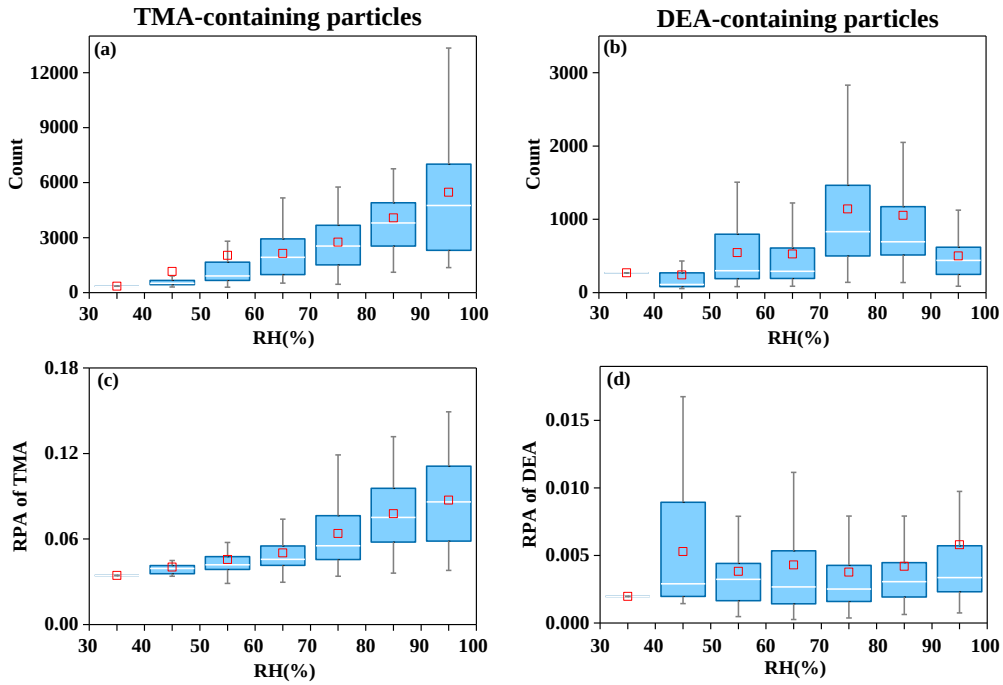

Figure 4. Particle counts of amine-containing particles and relative peak area (RPA) of the two amines in single particles, with an increase in ambient RH. (a, c) TMA-containing particles; (b, d) DEA-containing particles. Squares represent the average values. The line inside the box indicates the median. Upper and lower boundaries of the box represent the 75th and the 25th percentiles; the whiskers above and below each box represent the 95th and 5th percentiles.

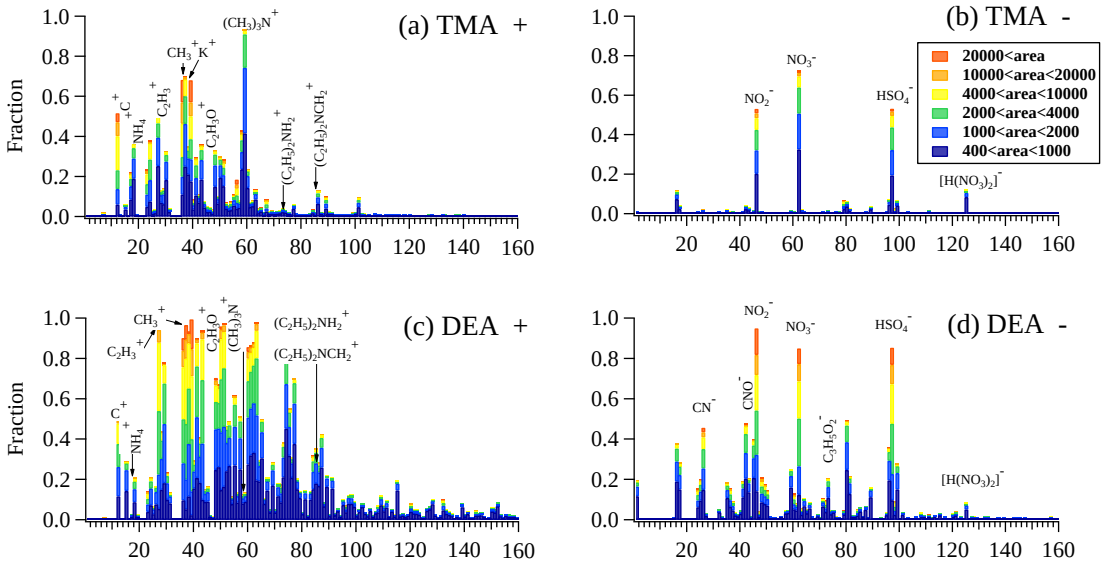

Figure 5. Mass spectra of TMA- and DEA-containing particles during the entire sampling period.

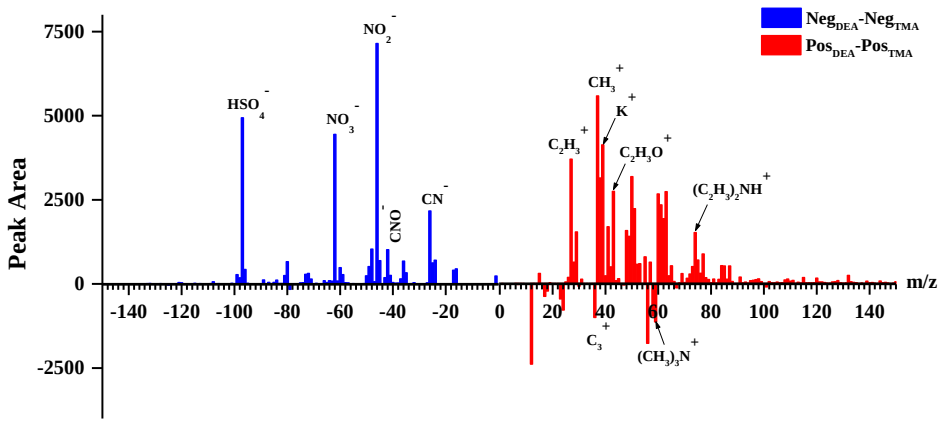

Figure 6. Differential mass spectra between DEA- and TMA-containing particles.

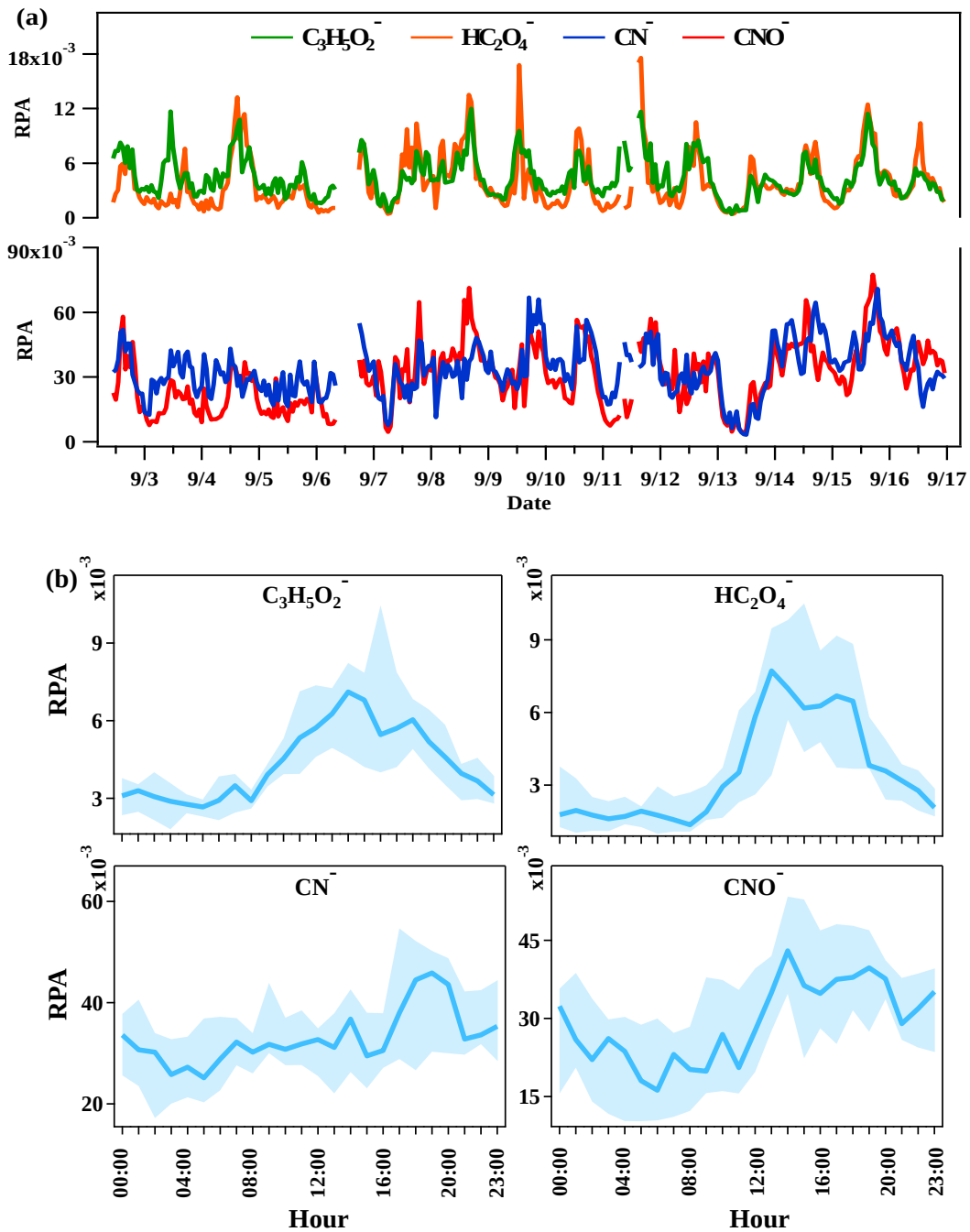

Figure 7. (a) Temporal trends of the relative peak areas (RPAs) of $^{73}C_3H_5O_2^-$, $^{89}HC_2O_4^-$, $^{26}CN^-$, and $^{42}CNO^-$ in DEA-containing particles. **(b)** Diurnal variations in the relative RPAs of $^{73}C_3H_5O_2^-$, $^{89}HC_2O_4^-$, $^{26}CN^-$, and $^{42}CNO^-$ in DEA-containing particles. The shaded areas represent the 75th and 25th percentiles.

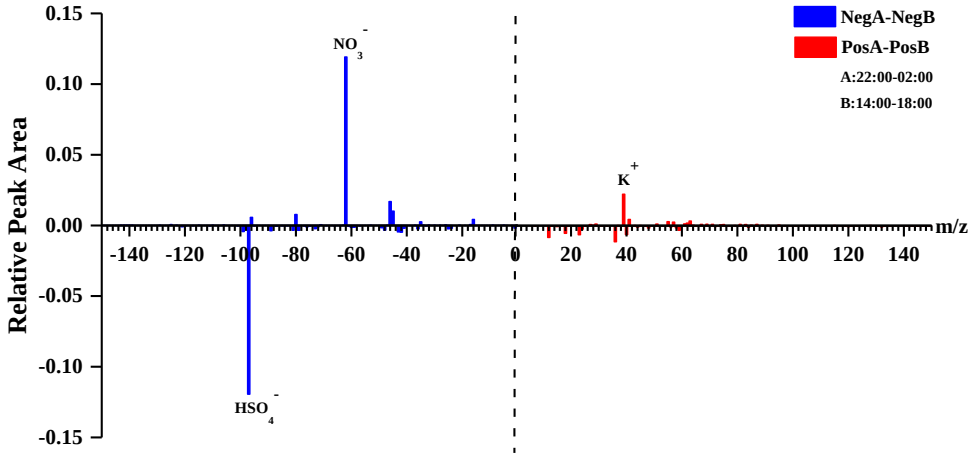

Figure 8. Differential mass spectra of DEA-containing particles between 22:00–02:00 and 14:00–18:00.

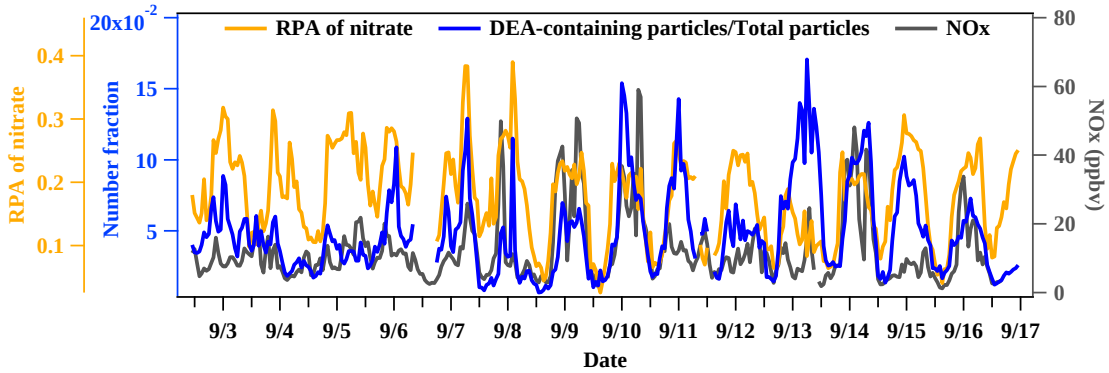

Figure 9. Temporal trends of RPA nitrate in DEA-containing particles, number fraction of DEA-containing particles in total particles, and NOx concentration.

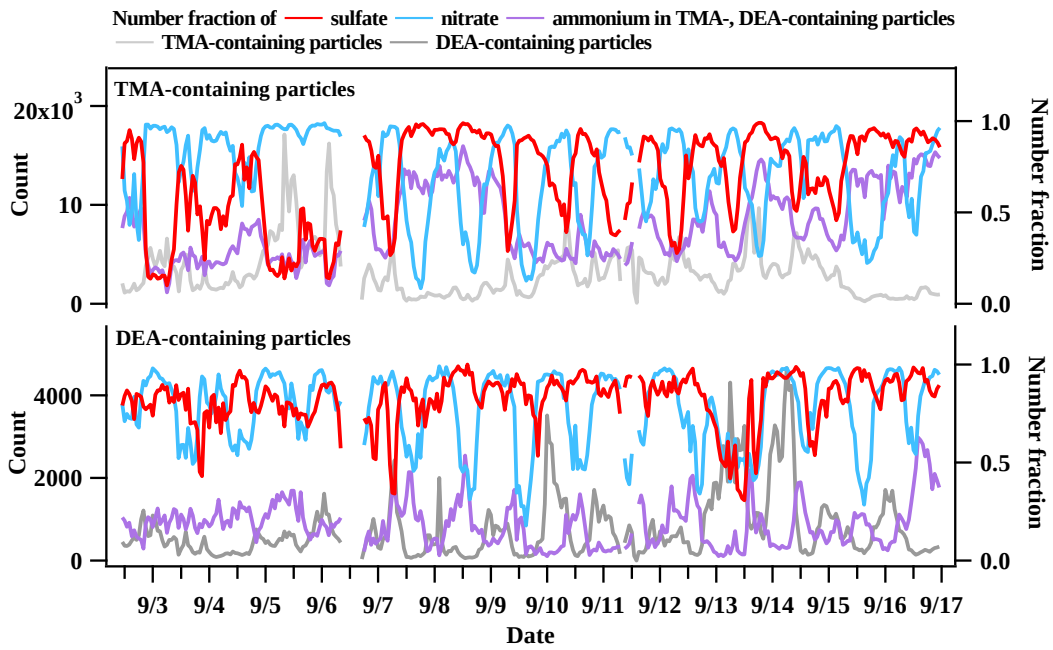

Figure 10. Temporal trends of TMA- and DEA-containing particle counts, and number fractions of nitrate, sulfate, and ammonium in TMA- and DEA-containing particles.

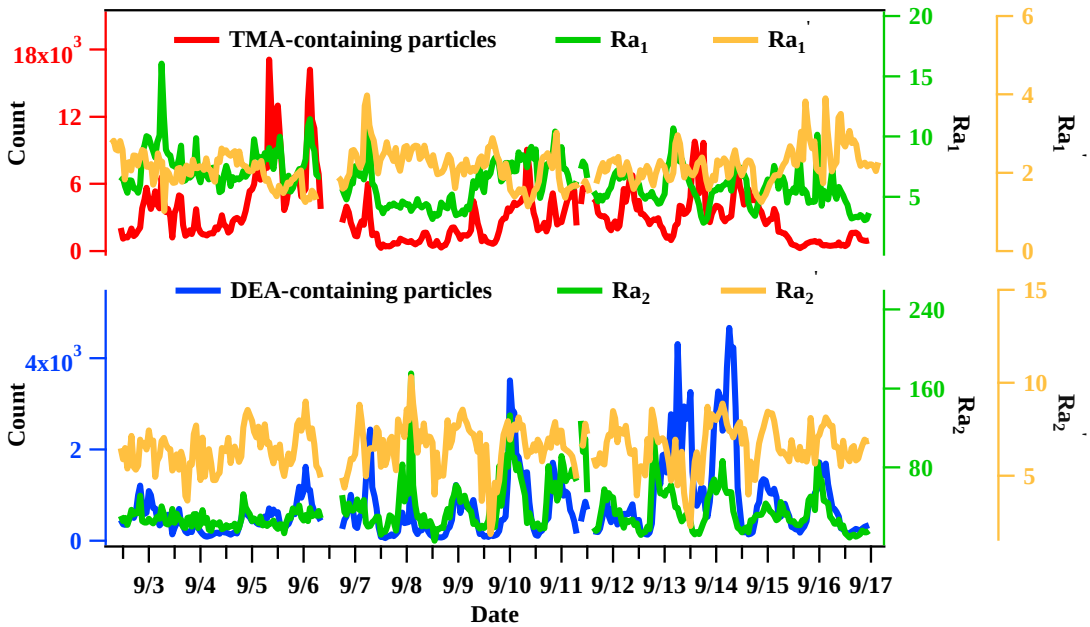

Figure 11. Temporal trends of the relative acidity ratios (Ra, Ra') in TMA- and DEA-containing particles.